Electronic Supplementary Material (ESI) for Catalysis Science & Technology.

Catalytic transfer hydrogenation of biomass-derived 5-hydroxymethylfurfural into 2,5-bis(hydroxymethyl)furan over tunable Zr-based bimetallic catalyst

Junnan Wei, Xuejuan Cao, Ting Wang, Huai Liu, Xing Tang, Xianhai Zeng, Yong Sun, Tingzhou Lei, Shijie Liu, Lu Lin**

MS patterns

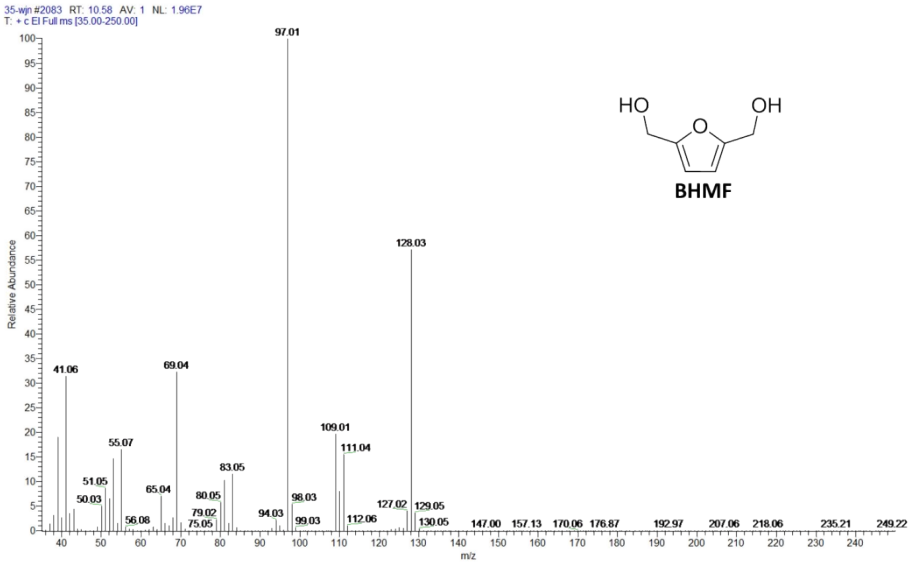

Figure S1. MS pattern of BHMF.

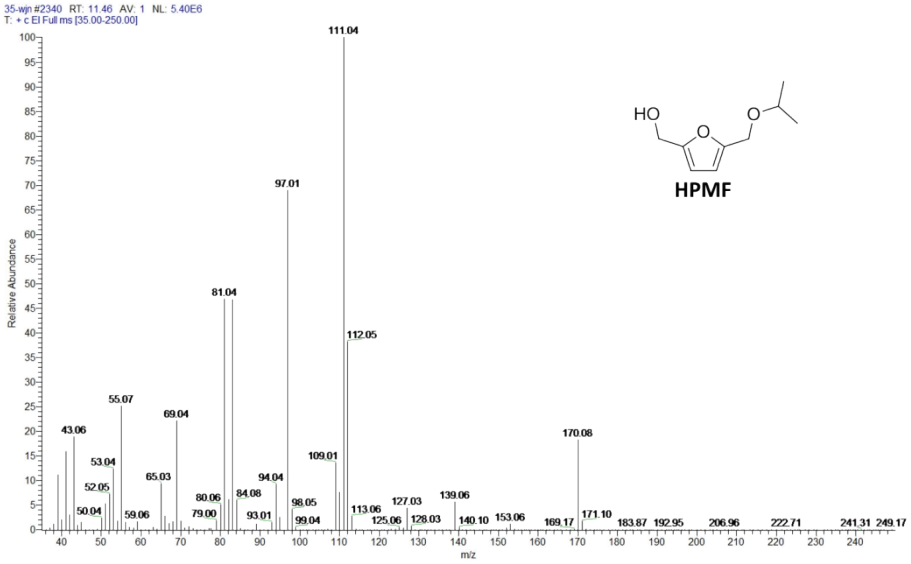

Figure S2. MS pattern of HPMF.

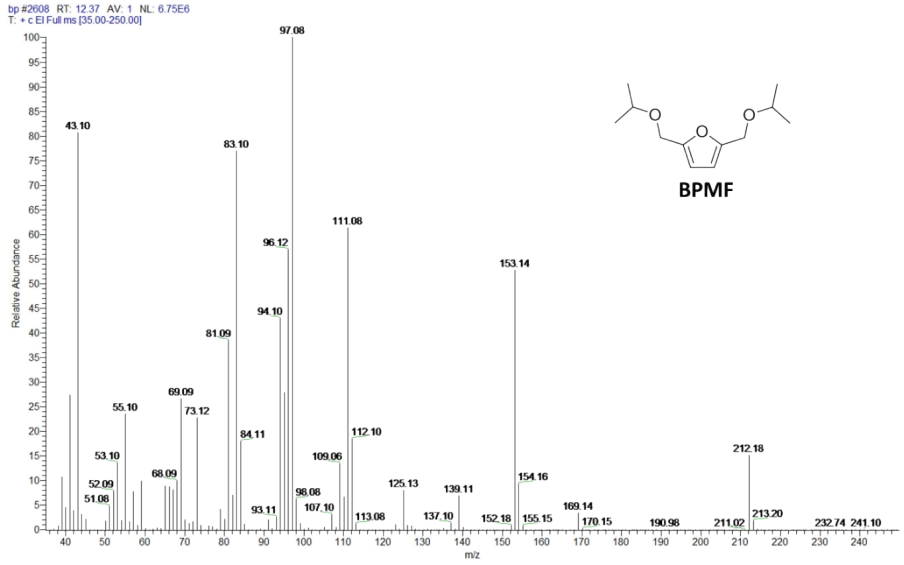

Figure S3. MS pattern of BPMF.

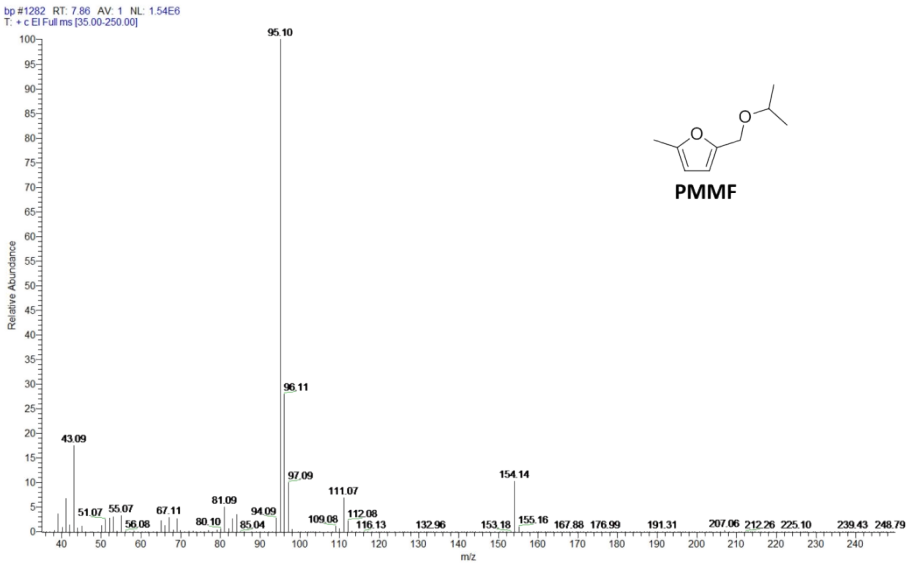

Figure S4. MS pattern of MPMF.

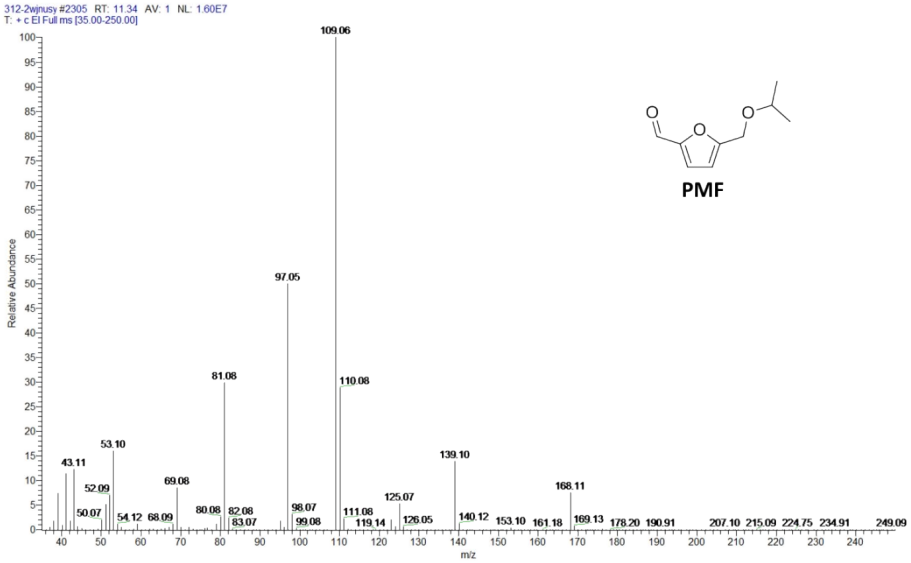

Figure S5. MS pattern of PMF.

Basic/acidic sites

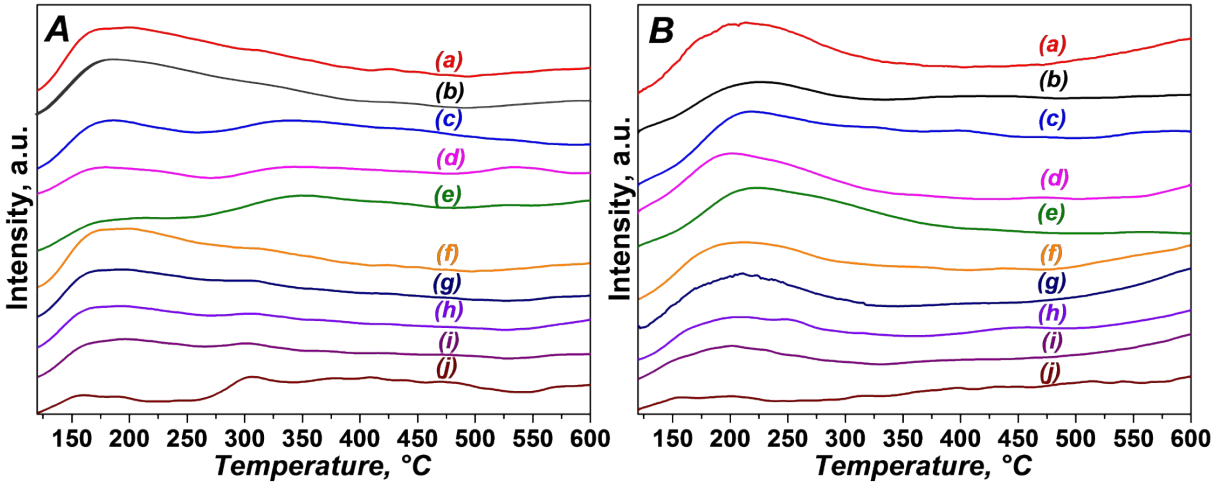

Figure S6. CO_2-TPD (A) and NH_3-TPD (B) profiles for Zr-SBA (a), Zr_{20}-SBA (b), ZrAl(1)-SBA (c), ZrCa(1)-SBA (d), ZrZn(1)-SBA (e), ZrBa(5)-SBA (f), ZrBa(3)-SBA (g), ZrBa(1)-SBA (h), ZrBa(1/3)-SBA (i) and Ba-SBA (j).

Table S1. Composition and acidic properties of Zr-SBA and ZrBa(3)-SBA.

Entry	Catalyst	Lewis sites[a], μmol/g	Brønsted sites[b], μmol/g	L/B[c]
1	Zr-SBA	67.7	6.0	11.3
2	ZrBa(3)-SBA	25.3	0.7	36.1

[a] Calculated by fitting deconvolution of peaks around at 1446 cm^{-1} in Figure 2. [b] Calculated by fitting deconvolution of peaks around at 1546 cm^{-1} in Figure 2. [c] The ratio of Lewis sites and Brønsted sites.

The role of the second metal oxide in Zr-based bimetallic catalysts

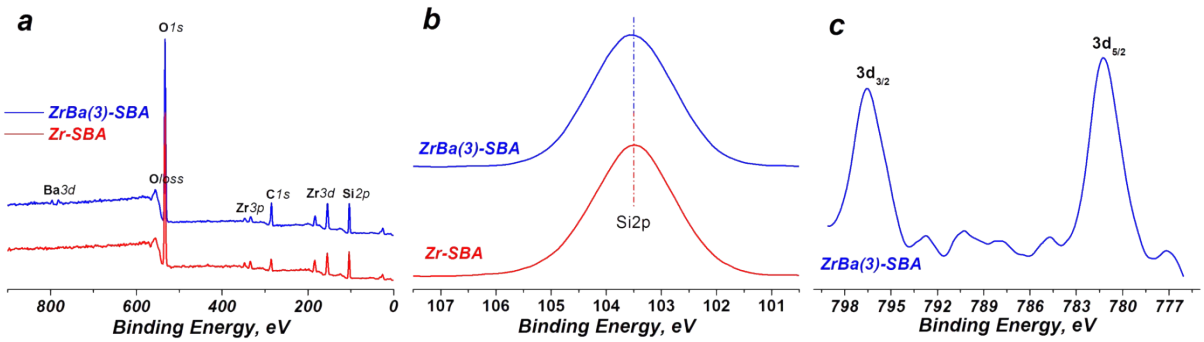

Figure S7. XPS spectra of ZrBa(3)-SBA and Zr-SBA: survey scan (a), high-resolution Si 2p (b) and Ba 3d (c).

In Figure S7, Zr-SBA and ZrBa(3)-SBA showed the same Si 2p binding energy (BE) value around at 103.5 eV. For ZrBa(3)-SBA, BE values centered at 781.3 and 796.5 eV were attributed to $3d_{5/2}$ and $3d_{3/2}$ spin-orbit components of Ba 3d, respectively.

The other physicochemical properties of ZrBa-SBA catalysts

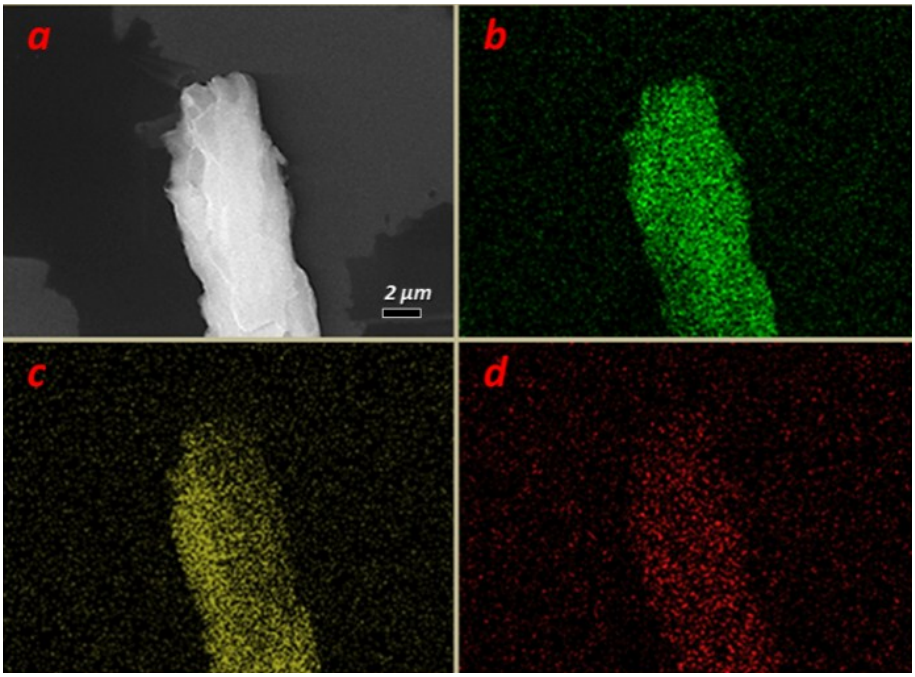

Figure S8. Electronic image (a), and O (b), Zr (c) and Ba (d) elemental mappings of ZrBa(3)-SBA.

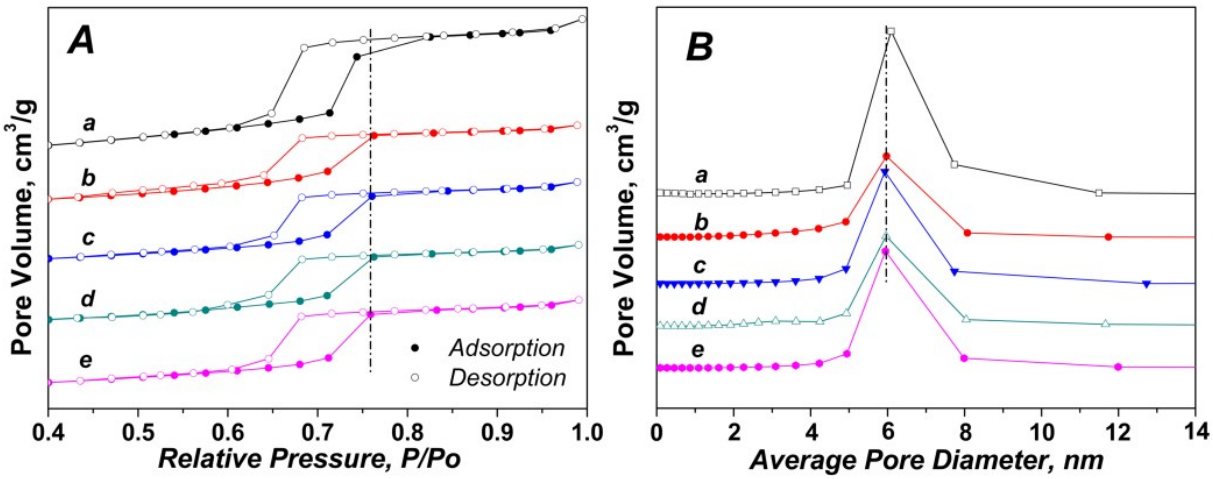

Figure S9. N_2 adsorption-desorption isotherms (A) and pore size distribution (B) of SBA-15 zeolite and variousZr-based catalysts: SBA-15 (a), Zr-SBA (b), ZrBa(1)-SBA (c), ZrBa(1/3)-SBA (d) and ZrBa(3)-SBA (e).

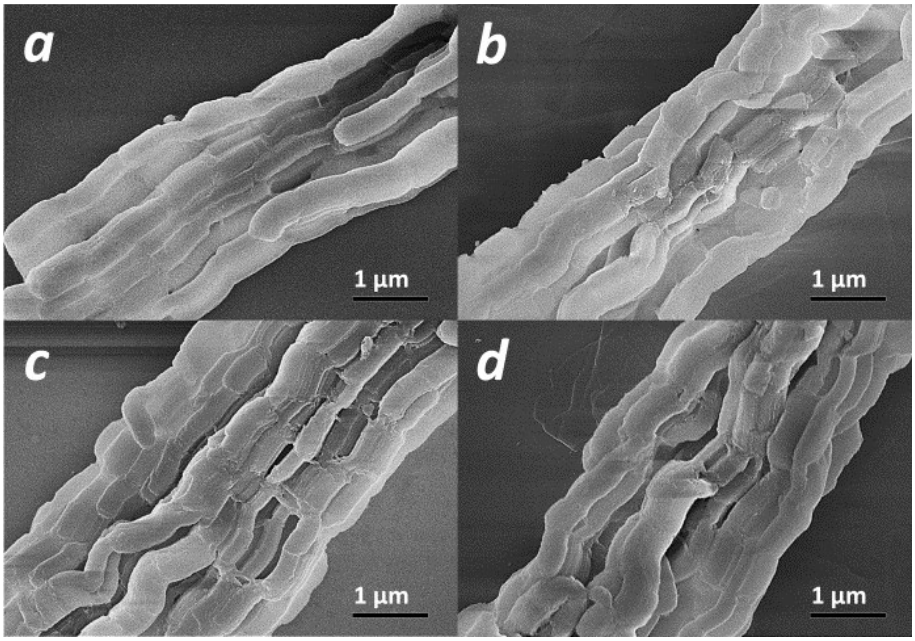

Figure S10. SEM images for SBA-15 zeolite (a), ZrBa(1/3)-SBA (b), ZrBa(1)-SBA (c) and ZrBa(3)-SBA (d).

Repeatability of experiments

Table S2. Repeatability tests of optimal results for yielding BPMF and BHMF.

Entry	Catalyst	T, ºC	T, h	X_{HMF}, %	Selectivity of products, %			
					BHMF	HPMF	BPMF	MPMF
1	Zr-SBA	180	4	100	nd	nd	87.6	7.8
2	Zr-SBA	180	4	100	nd	2.2	85.7	7.4
3	Zr-SBA	180	4	100	nd	nd	87.2	8.1
4	ZrBa(3)-SBA	150	2.5	98.3	92.2	7.1	nd	nd
5	ZrBa(3)-SBA	150	2.5	94.3	91.9	7.5	nd	nd
6	ZrBa(3)-SBA	150	2.5	96.6	91.3	7.6	nd	nd

Reaction conditions: 0.2 g HMF, 0.1 g catalyst for entries 1-3 or 0.2 g catalyst for entries 4-6, 19.8 g isopropanol and N_2 at atmospheric conditions; nd: not detected.

Characterizations for the spent catalysts

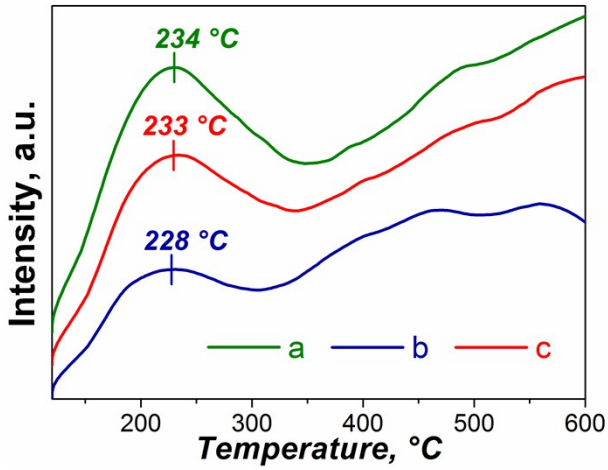

Figure S11. NH_3-TPD profile for the spent ZrBa(3)-SBA after the cycle 1 (a), the spent ZrBa(3)-SBA after the cycle 5 (b) and the regenerated ZrBa(3)-SBA(c).

Table S3. Various properties of the fresh, spent and regenerated catalysts.

Cycle	Fresh	1	5	Regenarated
V_{pore}[a], cm^3/g	0.50	0.47	0.45	0.47
D_{pore}[b], nm	5.7	5.7	5.6	5.7

[a] Total pore volume measured at P/P_0= 0.9999. [b] Average pore width calculated by BJH method.

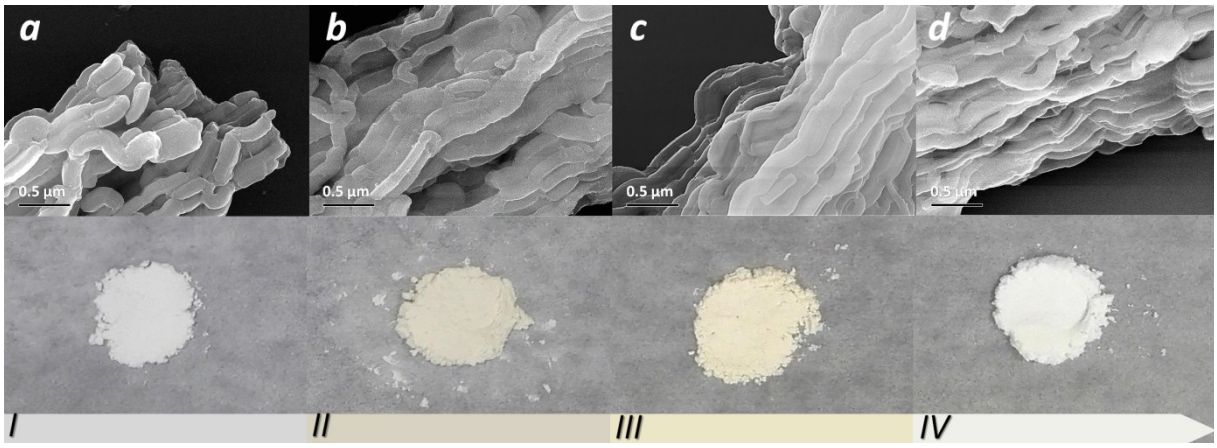

Figure S12. SEM images for the fresh ZrBa(3)-SBA (a), the spent ZrBa(3)-SBA after cycle 1 (b), the spent ZrBa(3)-SBA after cycle 5 (c) and the regenerated ZrBa(3)-SBA after cycle 5 (d).

NMR of purified BPMF

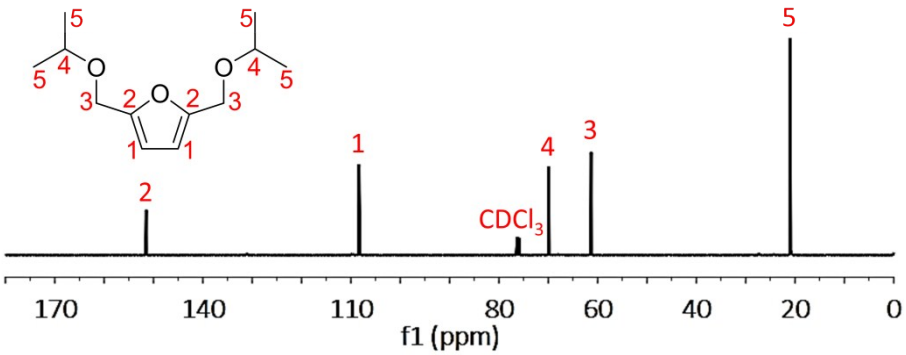

Figure S13. ^{13}C NMR $_{(CDCl3)}$ of purified BPMF.

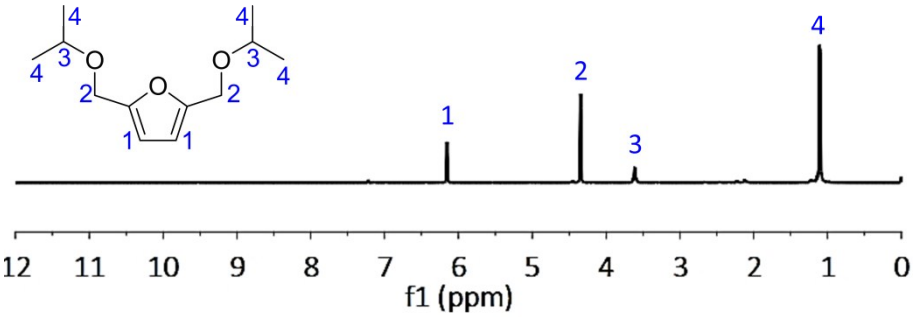

Figure S14. ^{1}H NMR $_{(CDCl3)}$ of purified BPMF.